Hetero-Nanonet Rechargeable Paper Batteries: Toward Ultrahigh Energy Density and Origami Foldability

Sung-Ju Cho, Keun-Ho Choi, Jong-Tae Yoo, Jeong-Hun Kim, Yong-Hyeok Lee, Sang-Jin Chun, Sang-Bum Park, Don-Ha Choi, Qinglin Wu, Sun-Young Lee, and Sang-Young Lee**

Forthcoming smart energy era is in strong pursuit of full-fledged rechargeable power sources with reliable electrochemical performances and shape versatility. Here, as a naturally abundant/environmentally friendly cellulose-mediated cell architecture strategy to address this challenging issue, a new class of hetero-nanonet (HN) paper batteries based on 1D building blocks of cellulose nanofibrils (CNFs)/multiwall carbon nanotubes (MWNTs) is demonstrated. The HN paper batteries consist of CNF/MWNT-intermingled heteronets embracing electrode active powders (CM electrodes) and microporous CNF separator membranes. The CNF/MWNT heteronet-mediated material/structural uniqueness enables the construction of 3D bicontinuous electron/ion transport pathways in the CM electrodes, thus facilitating electrochemical reaction kinetics. Furthermore, the metallic current collectors-free, CNF/MWNT heteronet architecture allows multiple stacking of CM electrodes in series, eventually leading to user-tailored, ultrathick (i.e., high-mass loading) electrodes far beyond those accessible with conventional battery technologies. Notably, the HN battery (multistacked $LiNi_{0.5}Mn_{1.5}O_4$ (cathode)/multistacked graphite (anode)) provides exceptionally high-energy density (=226 Wh kg^{-1} per cell at 400 W kg^{-1} per cell), which surpasses the target value (=200 Wh kg^{-1} at 400 W kg^{-1}) of long-range (=300 miles) electric vehicle batteries. In addition, the heteronet-enabled mechanical compliance of CM electrodes, in combination with readily deformable CNF separators, allows the fabrication of paper crane batteries via origami folding technique.

1. Introduction

Forthcoming smart energy era, which includes electric vehicles, grid-scale energy storage systems, and flexible/wearable electronics, is in strong pursuit of rechargeable power sources with reliable electrochemical performances and versatile form factors.[1] Among a wide variety of energy storage systems, current state-of-the-art lithium-ion batteries have undoubtedly occupied a predominant position in portable electronics and are now eager to extend their applications toward large-scale power source systems.[2] Since the commercialization of lithium-ion batteries by Sony in 1991, most research approaches reported to date have still relied on traditional synthetic materials and stereotyped electrode structure (i.e., thickness-directional, simple pile-up of electrode active materials/conductive additives/polymeric binders on top of metallic current collectors),[2,3] which have posed a major obstacle to sustainable/innovative progress of the batteries. For example, the presence of electrochemically inert materials such as metallic current collectors and polymer binders exerts negative influence on volumetric/gravimetric capacity of electrodes. In addition, the monotonous electrode architecture often gives rise to electrode thickness-dependent irregularity of electronic/ionic conduction pathways and also loss of structural integrity upon external deformation stress. In particular, the sluggish and nonuniform electron/ion transport provokes unwanted electrochemical polarization of cells, which becomes serious under harsh operating conditions such as high-mass loading electrodes[4] and fast charge/discharge reaction.[5]

As an eco-friendly 1D building element for use in paper electronics and paper batteries, cellulose nanofibrils (CNFs), a core constituent of cellulose obtained from naturally abundant/renewable wood and plants, have recently garnered a great deal of attention due to their peculiar characteristics such as lightweight, low-cost, physicochemical robustness, and recyclability.[6] Representative examples of CNFs in battery applications include: alternative electrode binders,[7] mechanical

S.-J. Cho, K.-H. Choi, J.-T. Yoo, J.-H. Kim, Y.-H. Lee, Prof. S.-Y. Lee, Dr. S.-Y. Lee
Department of Energy Engineering
School of Energy and Chemical Engineering
Ulsan National Institute of Science and Technology (UNIST)
Ulsan 689-798, South Korea
E-mail: syleek@unist.ac.kr; nararawood@forest.go.kr

S.-J. Chun, S.-B. Park, D.-H. Choi, Prof. S.-Y. Lee, Dr. S.-Y. Lee
Department of Forest Products
Korea Forest Research Institute
Seoul 130-713, South Korea

Prof. Q. Wu
School of Renewable Natural Resources
Louisiana State University Agricultural Center
Baton Rouge, LA 70803, USA

DOI: 10.1002/adfm.201502833

buffer of metallic anodes,[8] porous current collectors,[4b,9] and separator membranes.[10] Recently, Leijonmarck et al. fabricated the single-paper lithium-ion batteries using sequential filtration steps.[11] However, the use of Super-P powders as carbon conductive additives and inadequate dispersion of electrode slurries led to the unsatisfactory level of electrochemical performance and mechanical flexibility. Meanwhile, cellulose (or textile)/carbon nanotubes (CNTs) mixtures have been investigated as electroconductive scaffolds for use in binder-free/metallic current collector-free electrode systems.[4b,12] However, most of the previous works were focused on the development of CNTs-treated porous cellulose substrates, which were prepared by simple dipping/drying processes. A critical shortcoming of these electroconductive scaffolds is the low mass loading of electrode active materials, because pores of the preformed scaffolds are only space available for accommodating electrode active materials.

Here, as a 1D material-mediated cell architecture strategy to address the longstanding challenges of stereotypically structured conventional batteries and cellulose-based ones mentioned above, we demonstrate a new class of hetero-nanonet (HN) paper batteries based on 1D building blocks of CNFs/multiwall carbon nanotubes (MWNTs). The HN paper batteries proposed herein consist of CNF/MWNT-intermingled heteronets embracing electrode active powders (referred to as "CM electrodes") and microporous CNF separator membranes. The CNFs exhibit multifunctional roles as 1D electrode binders and also nanobuilding blocks for separator membranes. The MWNTs in the CM electrodes act as highly interconnected electronic networks and also alternative current collectors. Notably, the CNF/MWNT heteronet-enabled fiber tenacity contributes to securing structural robustness of CM electrodes without the aid of typical synthetic polymer binders (such as polyvinylidene fluoride (PVdF) and polytetrafluoroethylene (PTFE)), and metallic current collectors.

The HN paper batteries, by virtue of the CNF/MWNT heteronets-mediated CM electrodes and also the highly porous/readily deformable CNF separators, enable unprecedented improvements in the energy density and mechanical flexibility far beyond those achievable with conventional battery technologies. First, from the point of view of electronic/ionic transport kinetics, which is an indispensable prerequisite to ensure desirable electrochemical performances,[13] the 1D CNF/MWNT heteronets of CM electrodes create highly reticulated CNT networks and also interstitial voids (acting as ion-conducting channels after being filled with liquid electrolytes), eventually leading to the formation of 3D bicontinuous electron/ion conduction pathways. Second, the CM electrodes do not use metallic current collectors that are essentially required for conventional electrodes, thus accommodating a larger amount of electrode active materials in fixed electrode volume. Furthermore, multiple stacking of CM electrodes in series can be realized, producing user-tailored, ultrathick electrodes (e.g., thickness ≈1400 μm, areal mass loading ≈90 mg cm^{-2}) with facile electronic/ionic conduction behavior. Notably, such architectural uniqueness and simplicity of the HN paper cells provide exceptionally high-energy density (=226 Wh kg^{-1} $cell^{-1}$ at 400 W kg^{-1} $cell^{-1}$), which surpasses the target value (=200 Wh kg^{-1} at 400 W kg^{-1}) of long-range (=300 miles) electric vehicle batteries. Third, the CM electrodes can adopt a wide diversity of electrode active materials, underlying their versatility and scalability as a platform electrode technology. Fourth, the mechanically compliant CM electrodes (enabled by the CNF/MWNT heteronets and the removal of less-pliant metallic current collectors), in combination with the readily deformable CNF separators, allow the fabrication of a paper crane battery (an extreme example representing exceptional multifoldability of batteries) via origami folding technique.

2. Results and Discussion

2.1. Urea-Assisted Fabrication of CM Electrodes and Their Structural Uniqueness

The CNF suspension was obtained from the repeated high-pressure homogenization of wood cellulose powders in 5 wt% NaOH aqueous solution (Supporting Information, Figure S1a).[10,14] The dimension of CNFs is characterized with nanoscale diameter and length up to a few micrometers. Meanwhile, the MWNTs were subjected to ultrasonification in water, producing well-dispersed MWNT suspension (Supporting Information, Figure S1b), wherein 1 wt% sodium dodecyl sulfate (SDS) was incorporated as MWNT-dispersing agent.[15] A prerequisite condition for the fabrication of CM electrodes is to ensure the homogeneous dispersion of CNFs and MWNTs in the presence of electrode active materials. It is known[16] that strong intermolecular hydrogen bonding (arising from β-(1->4)-D-glucopyranose repeat units) of CNFs and also large difference in polarity between CNFs and CNTs make it difficult to attain uniform dispersion state of CNFs/CNTs mixtures in common solvents. Such poor dispersion state tends to become more serious as solid content of the mixture suspensions increases. Recently, Qi et al.[17] reported that urea additives in the NaOH aqueous solution effectively build chemical blocking between cellulose molecules and CNTs, thereby enabling the good dispersion of CNTs in the cellulose solution. Stimulated by these results, we incorporated urea additives into the CNF suspension in order to resolve the dispersion problem of CNF/MWNT mixture. As a preliminary experiment, a model system of CNFs (incorporating 1.5 wt% urea additive)/MWNTs (=15/85 (w/w)) mixture was fabricated and its wide-angle X-ray diffraction pattern was analyzed (**Figure 1**a). The CNF/MWNT mixture shows the characteristic peaks at $2\theta = 14.7°$ and 22.6°, which correspond to cellulose I crystalline form of CNFs with a good dispersion state.[18]

For the preparation of electrode mixture suspension, electrode active materials (here, $LiFePO_4$ (cathode) and $Li_4Ti_5O_{12}$ (anode) powders were chosen) were mixed with the MWNT suspension. Into the electrode materials/MWNTs mixture suspension, the CNF suspension containing the urea additive was added dropwise under vigorous stirring at 0 °C, producing the electrode mixture suspension (CNF/MWNT/electrode active materials = 5/15/80 (w/w/w) in aqueous solution). The optical microscopy images (Figure 1b) demonstrate the advantageous effect of urea additive on dispersion state of electrode ($LiFePO_4$)

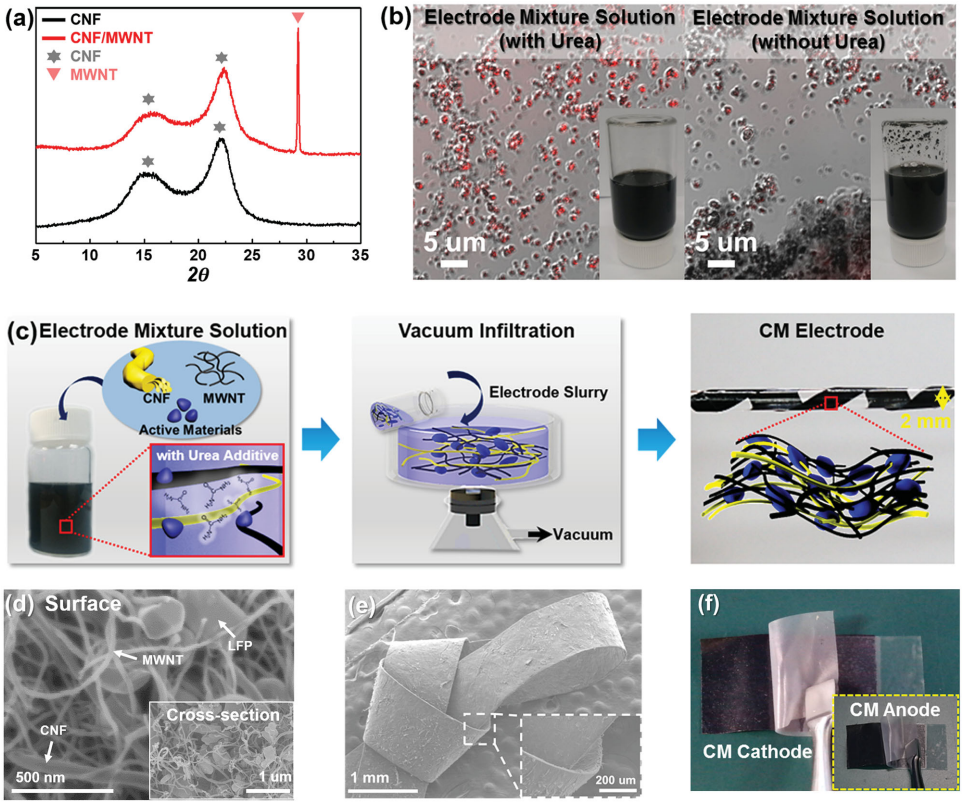

Figure 1. Fabrication and characterization of CM electrodes. a) X-ray diffraction patterns of CNF (incorporating 1.5 wt% urea additive)/MWNT mixture. b) Optical microscopy images showing the advantageous effect of urea additive on dispersion state of electrode mixture suspensions, wherein the CNFs were selectively stained with Congo red dye. The inset images show physical appearance of the electrode mixture suspensions. c) Schematic representations and photographs depicting the overall fabrication of CM electrodes. d) SEM images (surface and cross-section (=inset)) of CM $LiFePO_4$ cathode. e) SEM images showing mechanical flexibility of CM $LiFePO_4$ cathode. f) Photographs depicting structural integrity of CM electrodes after taping-out test.

mixture suspensions, with a particular focus on CNFs (represented by red dots, selectively stained with 0.5 wt% Congo red dye solution[19]. It is apparent that the electrode mixture suspension incorporating the urea additive exhibited the uniform dispersion of electrode components (i.e., CNFs, MWNTs, and $LiFePO_4$ powders), in comparison to a control suspension without urea additive. Such positive contribution of the urea additive was further verified by comparing the physical appearance of two electrode mixture suspensions (inset images of Figure 1b).

In contrast to conventional slurry coating-based electrodes, the CM electrodes were fabricated using vacuum-assisted infiltration technique analogous to papermaking process.[7b,11,14] The aforementioned electrode mixture suspension was poured onto a filter paper positioned inside a Porcelain Buchner funnel followed by vacuum infiltration, leading to the wet-state CM electrodes. Importantly, in order to promote the development of porous structure in the electrodes, the wet-state CM electrodes were subjected to solvent (ethanol followed by acetone) exchange-assisted freeze drying, eventually producing selfstanding/bendable CM electrodes. The effect of solvent exchange-assisted freeze drying on the porous structure and charge/discharge behavior of the CM electrodes was examined in detail (Supporting Information, Figure S2). The freeze-dried CM cathode (here, $LiFePO_4$ cathode was chosen) showed the well-developed porous structure (porosity ≈45%) than a control cathode that was not freeze-dried (porosity ≈22%), which thus exerted beneficial influence on the charge/discharge capacity and cell polarization. The overall fabrication procedure, along with the photographs representing each step, was depicted in a schematic illustration (Figure 1c).

The scanning electron microscopy (SEM) images (Figure 1d) show that the CNFs and MWNTs are well intermingled and generate the hetero-nanonets embracing $LiFePO_4$ powders. The uniform distribution of $LiFePO_4$ particles in the CM $LiFePO_4$ cathode, along with their relative composition ratio, was verified by conducting the energy dispersive X-ray spectroscopy analysis (Supporting Information, Figure S3), with a particular focus on Fe elements (represented by yellow dots). Notably, synthetic polymer binders, carbon powder conductive additives, and metallic current collectors, which are essentially used for conventional electrodes, were not observed in the CM $LiFePO_4$ cathode. Moreover, the CNF/MWNT-intermingled heteronets allow the formation of highly reticulated CNT networks and also interstitial voids (to be filled with liquid electrolytes), thus creating 3D bicontinuous electron/ion conduction pathways that can boost redox reaction kinetics of the CM $LiFePO_4$ cathode. The presence of MWNTs in the CM $LiFePO_4$ cathode

was also confirmed by the Raman spectra (Supporting Information, Figure S4). It is apparent that D (1346 cm^{-1}) and G (1583 cm^{-1}) bands corresponding to MWNTs[20] were observed at the CM $LiFePO_4$ cathode. The CNF/MWNT heteronet-mediated structural uniqueness was also found in the CM $Li_4Ti_5O_{12}$ anode (Supporting Information, Figure S5).

The CM electrodes can be wound along a glass rod (diameter = 2 mm, Figure 1c) and also knotted in the form of a ribbon without mechanical rupture (Figure 1e). The structural integrity of CM electrodes was examined using taping-out test with 3M scotch® tape. Figure 1f shows that neither peel-off nor disintegration of electrode components was found at the CM electrodes. This was further verified by analyzing the tape surfaces that were adjacent to the CM electrodes, after the taping-out test (Supporting Information, Figure S6). No detectable levels of electrode components detached from the CM electrodes were observed at the tape surfaces. This result demonstrates that the CNF/MWNT-intermingled heteronets hold electrode active materials tightly, even in the absence of synthetic polymer binders and metallic current collectors.

2.2. 3D Bicontinuous Electron/Ion Transport Phenomena of CM Electrodes and Their Influence on Electrochemical Performance

The structural novelty (specifically, CNF/MWNT-intermingled heteronet embracing electrode active materials) of CM electrodes plays a key role in the construction of 3D bicontinuous electron/ion transport pathways (**Figure 2**a). At a fixed $LiFePO_4$ content level (=80 wt%), the electronic conductivity of CM cathodes tends to increase with the MWNT content (Supporting Information, Figure S7a). However, a higher MWNT content (i.e., corresponding to a lower CNF content) exerted a harmful influence on structural stability of CM $LiFePO_4$ cathodes (Supporting Information, Figure S7b). Taking into account this trade-off behavior between electronic conductivity and structural stability, the desirable content of MWNTs in the CM $LiFePO_4$ cathodes was controlled at 15 wt%. Figure 2b shows that the CM electrodes present higher electronic conductivities (cathode = 4.2 S cm^{-1} and anode = 11.8 S cm^{-1}) than the conventional ones (cathode ($LiFePO_4$/PVdF/carbon black = 80/10/10 (w/w/w)) = 0.5 S cm^{-1}, anode ($Li_4Ti_5O_{12}$/PVdF/carbon black = 88/10/2 (w/w/w)) = 0.3 S cm^{-1}). Such a higher electronic conductivity of the CM electrodes is attributed to the well-interconnected electronic networks of MWNTs and also the removal of synthetic polymer binders (such as PVdF) that partially shield electrode active materials and conductive additives.

The CM electrodes show a higher porosity than the conventional ones (45% (CM $LiFePO_4$ cathode)/41% (CM $Li_4Ti_5O_{12}$ anode) versus 20% (conventional $LiFePO_4$ cathode)/18% (conventional $Li_4Ti_5O_{12}$ anode), Figure 2b). This improvement in the porosity of CM electrodes can be explained by the spatially reticulated interstitial voids formed between the 1D nanobuilding blocks of CNF/MWNT. In addition, the polar CNFs in the CM electrodes are beneficial for facilitating capillary intrusion of liquid electrolyte,[10] leading to better electrolyte wettability than the conventional electrodes (Figure 2b and Figure S8 (Supporting Information)). These well-established and polar porous channels (that allow facile accessibility of liquid electrolyte), in combination with the aforementioned MWNT electronic networks, help boost up electrochemical reaction kinetics of the CM electrodes.

The charge/discharge performance of the CM $LiFePO_4$ cathodes was explored using a coin-type half cell (composed of $LiFePO_4$ cathode/Li metal). Figure 2c shows that the CM $LiFePO_4$ cathode delivers the higher specific gravimetric discharge capacity (≈167 mAh g^{-1}) than the conventional $LiFePO_4$ cathode (≈153 mAh g^{-1}) at charge/discharge current density of 0.2 C/0.2 C under voltage range of 2.0–4.0 V, which appears closer to the theoretical value (≈170 mAh g^{-1}) of $LiFePO_4$ active materials.[21] Intriguingly, the capacity originating from the MWNTs themselves, which was measured from a model electrode (MWNT/CNF = 85/15 (w/w), without $LiFePO_4$ powders), was found to be negligibly small (Supporting Information, Figure S9) compared to that of the CM $LiFePO_4$ cathode. This result reveals that the relatively higher discharge capacity (shown in Figure 2c) of the CM $LiFePO_4$ cathode could be ascribed to its structural excellence (i.e., 3D bicontinuous electron/ion conduction pathways)-driven facilitation of the Faradaic reaction kinetics.

Over a wide range of discharge current densities (=0.2–30.0 C, at a fixed charge current density of 0.2 C), the CM $LiFePO_4$ cathode shows significant improvement in the specific gravimetric discharge capacities (Figure 2d and Figure S10 (Supporting Information)) and also mitigation in the cell polarization (Figure 2e) than the conventional one, demonstrating the electrochemical superiority of the CM $LiFePO_4$ cathode in the rate capability of cells. This faster rate performance of the CM $LiFePO_4$ cathode was verified by conducting the Galvanostatic Intermittent Titration Technique (GITT) analysis[22] (Figure 2f). The CM $LiFePO_4$ cathode effectively alleviates the build-up in cell polarization upon the repeated current stimuli (at current density = 2.0 C, interruption time between each pulse = 3 min) during charge/discharge reaction. The internal cell resistances are summarized as a function of state of charge and also depth of discharge (insets of Figure 2f). In addition to the rate capability, the cycling performance (at charge/discharge current density = 1.0 C/1.0 C) of the CM $LiFePO_4$ cathode was examined. Even after 500 cycles, the CM $LiFePO_4$ cathode presents the higher capacity retention (≈95%) than the conventional $LiFePO_4$ cathode (≈91%) (Figure 2g and Figure S11 (Supporting Information)).

It is underlined again that the CM electrodes necessitate neither synthetic polymer binders nor metallic current collectors, which thus allows larger amount of electrode active materials to be loaded in a fixed electrode volume. At a similar cathode thickness (≈60 μm), the areal mass loading (calculated solely by $LiFePO_4$ mass) of the CM $LiFePO_4$ cathode (=4.4 mg $cm_{cathode}^{-2}$) was approximately two times larger than that (=2.3 mg $cm_{cathode}^{-2}$) of the conventional $LiFePO_4$ cathode, eventually contributing to a substantial increase in the discharge capacity per cathode area (0.68 mAh $cm_{cathode}^{-2}$ for the CM $LiFePO_4$ cathode versus 0.35 mAh $cm_{cathode}^{-2}$ for the conventional $LiFePO_4$ cathode, Figure S12 (Supporting Information) and Figure 2h).

2.3. Thickness-Tunable/Multistackable CM Electrodes for Ultrahigh Energy Density Cells

The selfstanding, ultrathick (thickness ≈1400 μm) CM $LiFePO_4$ cathode was successfully fabricated without impairing its

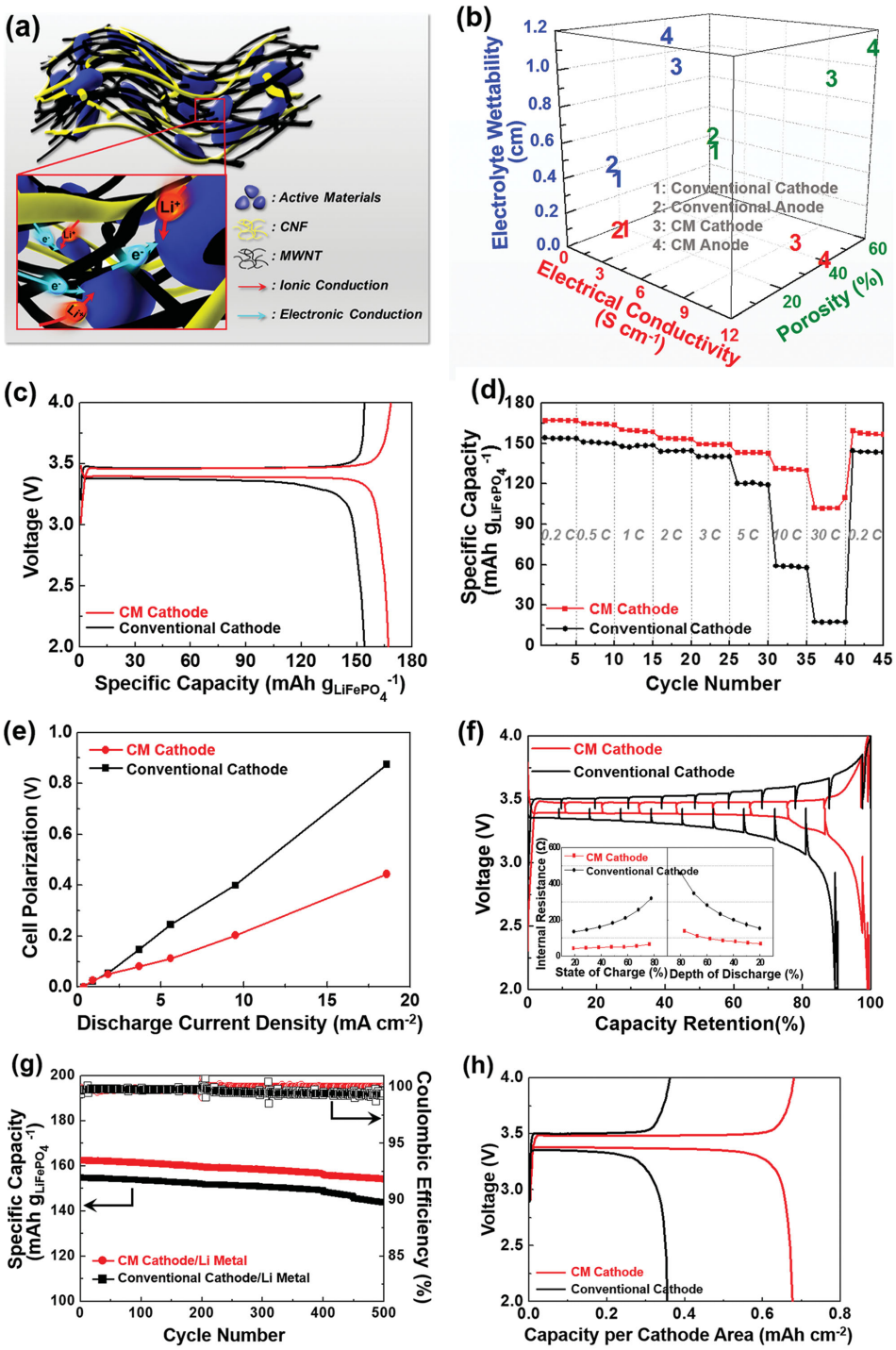

Figure 2. 3D bicontinuous electron/ion transport phenomena of CM electrodes. a) A schematic illustration depicting CNF/MWNT-intermingled heteronet architecture of CM electrodes. b) Comparison in electronic conductivity, porosity, and electrolyte wettability (CM electrodes versus conventional ones). c) Charge/discharge profiles of CM cathode or conventional cathode. d–h) Comparison in cell performance (CM $LiFePO_4$ cathode versus conventional $LiFePO_4$ one): d) discharge rate capability over a wide range of discharge current densities at a fixed charge current density of 0.2 C; e) cell polarization obtained from average discharge potential as a function of discharge current density; f) GITT analysis, wherein, insets show the variation of internal cell resistance as a function of state of charge and depth of discharge; g) cycling performance (charge/discharge current density = 1.0 C/1.0 C, voltage range = 2.0–4.0 V); h) discharge capacity per cathode area (mAh $cm_{cathode}^{-2}$) under a similar cathode thickness.

dimensional stability (**Figure 3**a). By comparison, for the conventional $LiFePO_4$ cathode prepared by typical slurry coating process, the serious problem in structural integrity (specifically, detachment of electrode components from an aluminum current collector) was observed even at the cathode thickness of ≈500 µm (inset image of Figure 3a). The SEM images

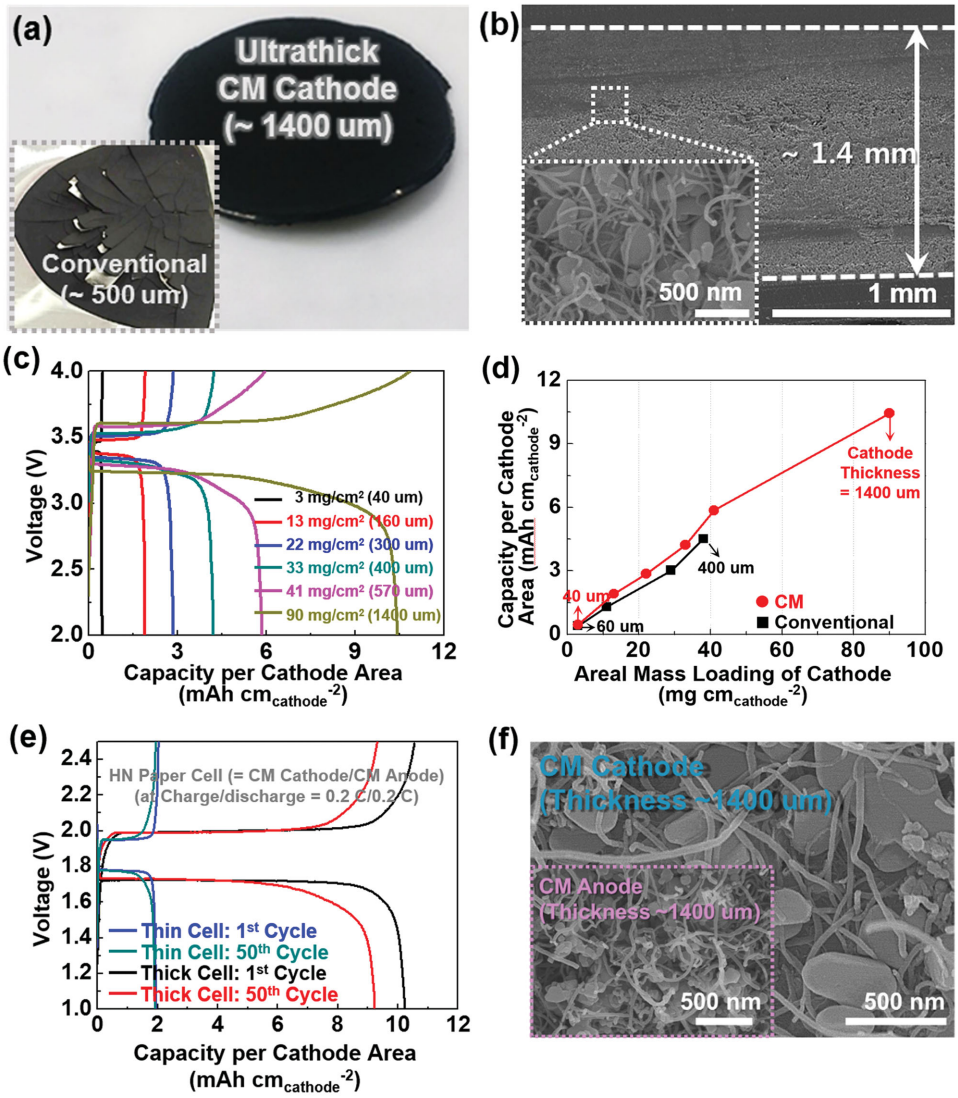

Figure 3. Morphology and electrochemical performance of thickness-tunable CM electrodes. a) A photograph depicting the self-standing, dimensionally tolerable ultrathick (thickness ≈ 1400 μm) CM cathode. An inset image shows the poor structural stability of the conventional cathode (thickness ≈ 500 μm). b) A SEM image (cross-section) of the ultrathick CM cathode (an inset image is the high-magnification view). c,d) Cell performance of thickness-tunable CM cathodes as a function of cathode thickness (i.e., areal mass loading): c) charge/discharge profiles of CM $LiFePO_4$ cathodes; d) comparison in capacity per cathode area (mAh $cm_{cathode}^{-2}$) between CM cathodes and conventional ones. e) Cycling performance of HN paper full cells (=CM $LiFePO_4$ cathode/CNF separator/CM $Li_4Ti_5O_{12}$ anode) as a function of electrode thickness. f) SEM images of CM cathode (thickness ≈ 1400 μm) and CM anode (thickness ≈ 1400 μm) in the HN paper full cell, after the cycling test.

(Figure 3b) of the ultrathick CM $LiFePO_4$ cathode exhibit that the CNF/MWNT heteronets, along with the $LiFePO_4$ powders, are uniformly distributed in the through-thickness direction, and also the spatially reticulated MWNT networks/interstitial voids are well developed (inset image of Figure 3b).

The half cell (assembled with ultrathick (≈1400 μm) CM $LiFePO_4$ cathode/Li metal anode) showed normal charge/discharge profiles at charge/discharge current density of 0.2 C/0.2 C (Figure 3c). The electrochemical performance of thickness-tunable CM $LiFePO_4$ cathodes was further examined by measuring discharge capacity per cathode area as a function of areal mass loading, which was simply controlled by varying the amount of electrode mixture suspension during the vacuum-assisted infiltration. The areal capacity tends to linearly increase with areal mass loading (Figure 3c,d). Notably, the thick CM $LiFePO_4$ cathode (thickness ≈ 1400 μm, areal mass loading ≈ 90 mg $cm_{cathode}^{-2}$) provides a remarkable increase in areal capacity (=10.5 mAh $cm_{cathode}^{-2}$), in comparison to the thin CM $LiFePO_4$ cathode (areal capacity ≈0.46 mAh $cm_{cathode}^{-2}$, thickness ≈ 40 μm, areal mass loading ≈ 3 mg $cm_{cathode}^{-2}$). It is known that the areal capacity of 10 mAh $cm_{electrode}^{-2}$ is a symbolic value[23] which corresponds to stripping/plating of a lithium layer with thickness 50 μm (on the basis of lithium metal electrode). Taking into account such a challenging goal, the CM electrode can provide a promising solution to address the high capacity issue of lithium-ion batteries. By comparison, the conventional $LiFePO_4$ cathode (Supporting Information, Figure S13) failed to exceed the areal mass loading of 38 mg $cm_{cathode}^{-2}$ (corresponding to the areal capacity of 4.5 mAh $cm_{cathode}^{-2}$).

Based on the structural/electrochemical understanding of the CM cathodes mentioned above, cycling performance (expressed as discharge capacity per cathode area) of HN paper full cells (comprising CM $LiFePO_4$ cathode/CNF separator/CM $Li_4Ti_5O_{12}$ anode) was examined, where the cell was cycled at charge/discharge current density of 0.2 C/0.2 C under voltage range of 1.0–2.5 V. Here, the CNF separator having labyrinth-like, highly porous structure (thickness ≈ 30 μm, porosity ≈ 48%; Figure S14 (Supporting Information)) was fabricated via the vacuum infiltration method,[4b,24] wherein 5.0 wt% silica nanoparticles were added as CNF disassembling agent to improve porosity of the CNF separator. The more details on the structure and properties of the CNF separator were described in the previous studies.[24]

The HN paper cells showed stable charge/discharge profiles during the cycling test (Figure 3e). Notably, the thick HN paper cell (containing CM $LiFePO_4$ cathode (≈1400 μm) and

CM $Li_4Ti_5O_{12}$ anode (≈1400 μm)) provided the substantially larger areal capacities than the thin HN paper cell (assembled with CM $LiFePO_4$ cathode (≈150 μm) and CM $Li_4Ti_5O_{12}$ anode (≈150 μm)), demonstrating the beneficial effect of the thick electrodes on the areal capacity of cells. Meanwhile, the cycling performance of the thick HN paper cell was slightly lower than that of the thin cell, which should be further improved in future studies. The morphological analysis (Figure 3f) exhibits that the CNF/MWNT hetero-nanonet structure of the ultrathick CM electrodes in the HN paper cell was well preserved after the cycling test, verifying its long-term structural/electrochemical durability.

The metallic current collectors-free CNF/MWNT heteronets are expected to allow multiple stacking of CM electrodes in series, eventually leading to user-tailored, ultrathick electrodes with reliable electrochemical performances. Here, in an attempt to develop ultrahigh energy density cells, high-voltage spinel $LiNi_{0.5}Mn_{1.5}O_4$[25] (as cathode material) and natural graphite powders (as anode material) were employed, instead of the previously used $LiFePO_4/Li_4Ti_5O_{12}$ system. Zhang and co-workers[26] reported similar stacked electrode structure, however, in comparison to the CNF/MWNT heteronet-based CM electrodes presented herein, the sulfur cathodes comprising sulfur-loaded MWNTs and vertically aligned CNTs produced the layer-by-layer lasagna-like structure. **Figure 4**a shows that a diversity of CM $LiNi_{0.5}Mn_{1.5}O_4$ cathodes in thickness is fabricated by simply controlling the number of cathode sheets (50 μm (1 sheet), 450 μm (10 sheets), 1300 μm (30 sheets)). The predetermined number of elementary cathode sheets was stacked in series and then subjected to roll pressing at room temperature to secure tightly interlocked interface between the adjacent elementary cathode sheets (e.g., 450 μm (10 sheets); Supporting Information, Figure S15). The discrepancy between the actual electrode thickness and the initially expected number of stacked sheets is attributed to the thickness-directional compression during the roll pressing. By exploiting this stackable electrode concept, we can easily fabricate exceptionally thick electrodes that are almost impossible to reach with conventional battery technologies. The discharge capacities per cathode area (mAh $cm_{cathode}^{-2}$) of the CM $LiNi_{0.5}Mn_{1.5}O_4$ cathodes tend to increase in proportion to their thickness (i.e., the number of elementary CM cathode sheets) (Figure 4b), where half cells ($LiNi_{0.5}Mn_{1.5}O_4$ cathode/Li metal) were examined at charge/discharge current density of 0.2 C/0.2 C under voltage range of 3.0–5.0 V.

To better understand the electrochemical behavior of the multistackable CM cathodes, overpotential distribution in their through-thickness direction was investigated in great detail using in situ electrochemical impedance spectroscopy (EIS) measurement based on electrode-by-electrode stack cell configuration.[27] In this cell configuration, each electrode layer is in ionic contact (i.e., allowing lithiation/delithiation reaction) but electronically isolated from the next electrode layer by a polyethylene separator. Thus, a working electrode positioned far away from a counter electrode may have difficulties in activating electrochemical reaction (thus, leading to serious polarization in charge/discharge profiles), as compared to that close to the counter electrode. In this study, a cathode with a thickness of 200 μm was chosen as a unit working electrode. Three cathode layers were stacked in series and a lithium metal disc was used as a counter/reference electrode (Supporting Information, Figure S16a). Figure 4c shows that the significant increase in overpotential (≈91 mV) was observed at the conventional $LiNi_{0.5}Mn_{1.5}O_4$ cathode, revealing the sluggish and nonuniform electronic/ionic flow in its through-thickness direction. For the conventional cathode, ionic transport is hindered by the presence of synthetic polymer binders. Also, construction of well-interconnected electronic conduction pathways is highly challenging due to the dispersion issue of carbon powder conductive additives as well as the electronic shielding by the polymer binders. By comparison, for the CM $LiNi_{0.5}Mn_{1.5}O_4$ cathode, the rise in overpotential (≈1.4 mV) was found to be negligibly small. Furthermore, the CM $LiNi_{0.5}Mn_{1.5}O_4$ cathode presents the larger areal discharge capacity (≈5.7 mAh $cm_{cathode}^{-2}$) than the conventional one (≈4 mAh $cm_{cathode}^{-2}$). Such a noteworthy improvement in the thickness-directional overpotential and also in areal discharge capacity could be attributed to the highly developed 3D bicontinuous electronic/ionic conduction pathways, which was conceptually illustrated in Figure S16b (Supporting Information).

A single-unit cell comprising solely one cathode sheet/one separator/one anode sheet,[28] instead of traditional cells fabricated by repeatedly winding or stacking cell components, is an ultimate cell configuration that rechargeable batteries are keen to achieve. This single-unit cell could simplify cell assembly processes and also benefit from the increase of cell capacity by minimizing the use of electrochemically inert components (such as metallic current collectors and separators). A conceptual representation of a single-unit cell and its beneficial contribution to cell capacity, along with the structural uniqueness of multistackable CM electrodes, is illustrated in Figure 4d.

Figure 4e shows that one sheet of multistacked CM $LiNi_{0.5}Mn_{1.5}O_4$ cathode (thickness ≈ 450 μm, prepared by stacking ten sheets of the elementary cathode (≈50 μm)) and one sheet of multistacked CM graphite anode (thickness ≈ 160 μm, 3 sheets of the elementary anode (≈60 μm)) are integrated with one sheet of CNF separator (≈30 μm), eventually leading to the formation of a single-unit HN paper full cell. The single-unit HN paper cell showed normal charge/discharge behavior and also areal (normalized by cathode area) discharge capacity of 4.78 mAh $cm_{cathode}^{-2}$ (Supporting Information, Figure S17). The cycling performance (expressed as a real capacity (mAh $cm_{cathode}^{-2}$)) of the single-unit HN paper cells was investigated (Figure 4e), where the cells were cycled at charge/discharge current density of 0.2 C/0.2 C under voltage range of 3.0–4.9 V. Both the thin cell (assembled with the elementary CM electrodes (cathode/anode ≈ 50/20 μm/μm)) and the thick cell (composed of the stacked CM electrodes (cathode/anode ≈ 450/160 μm/μm)) showed stable charge/discharge behavior with cycling (Figure 4e and Figure S18 (Supporting Information)), although the cycling performance of the thick cell was slightly lower than that of the thin cell. Meanwhile, the thickest cell (cathode/anode ≈ 1300/440 μm/μm) did not yet reach a satisfactory level of cycling performance, which should be improved in future studies by further tuning electrode structure and electrolyte additives.

The influence of the single-unit HN paper cells on the Ragone plot, where the gravimetric energy/power densities of cells were determined on the basis of cell mass (= cathode + anode + separator), was examined (Figure 4f). To highlight a

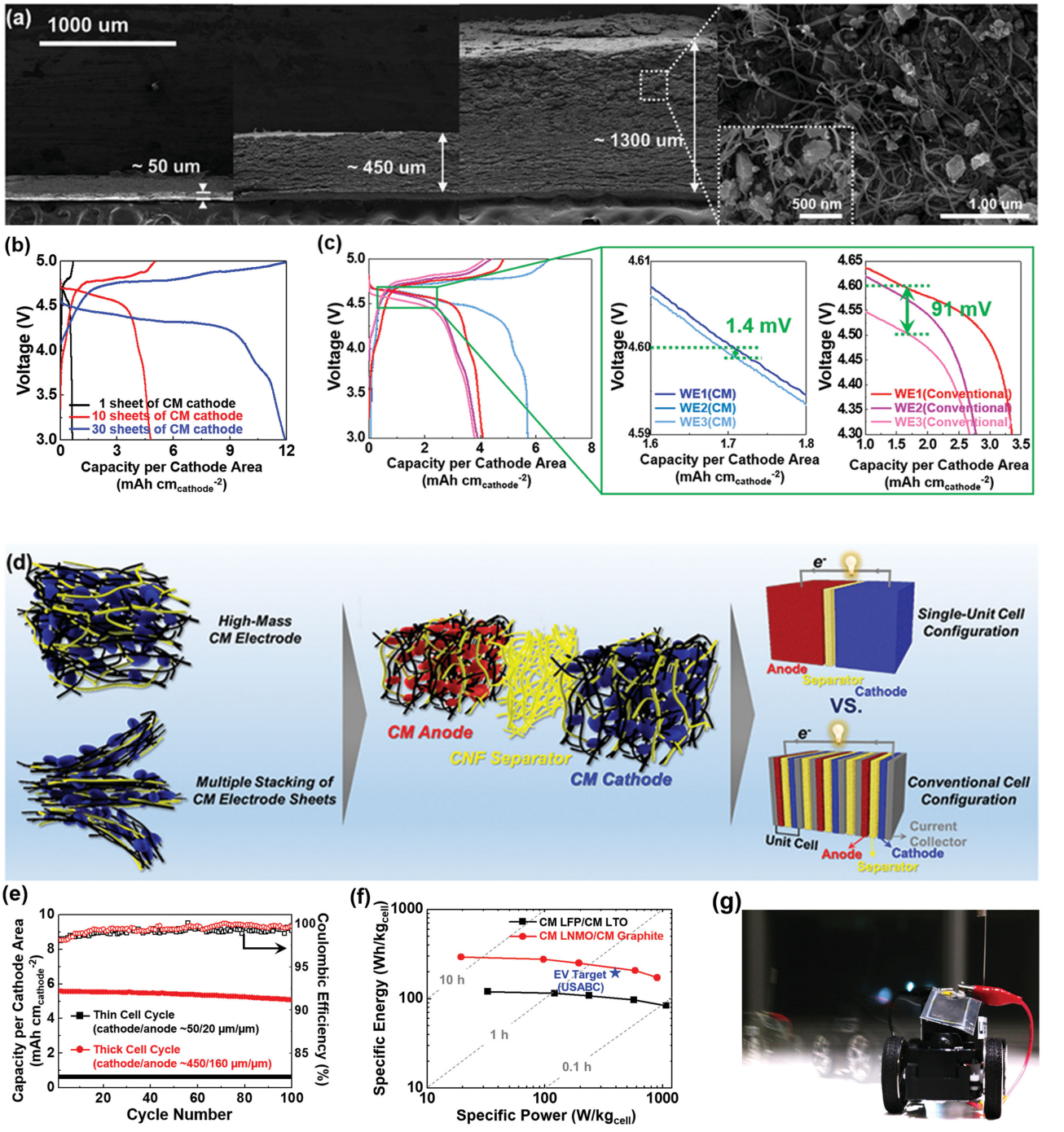

Figure 4. Structural/electrochemical uniqueness of multi-stackable CM electrodes. a) SEM images of multi-stacked CM $LiNi_{0.5}Mn_{1.5}O_4$ cathodes with various thickness (50 μm (1sheet), 450 μm (10 sheets), 1300 μm (30 sheets)). b) Discharge capacities per cathode area (mAh $cm_{cathode}^{-2}$) of CM $LiNi_{0.5}Mn_{1.5}O_4$ cathodes as a function of cathode thickness, where half cells (=$LiNi_{0.5}Mn_{1.5}O_4$ cathode/Li metal) were examined. c) Overpotential distribution in through-thickness direction of electrodes and areal discharge capacity (CM $LiNi_{0.5}Mn_{1.5}O_4$ cathode versus conventional one). d) A conceptual representation of a single-unit cell and its contribution to energy density of cells. e) Cycling performance of single-unit HN paper cells. f) Ragone plot of single-unit HN paper cells, where the gravimetric energy/power densities of cells were determined on the basis of cell mass (= cathode + anode + separator). g) A photograph showing the operation of a mini toy car installed with the single-unit HN paper cell.

noteworthy result of the single-unit HN paper cells, the target energy/power density values (=200 Wh kg^{-1}/400 W kg^{-1}) of long-range (=300 miles) EV batteries, which was announced by US Advanced Battery Consortium (USABC),[29] were also marked on the Ragone plot. Although the cell mass used herein is not completely same as that of the USABC target cells, it should be noted that the energy density of the single-unit HN paper cell (=226 Wh kg^{-1} at 400 W kg^{-1}, CM $LiNi_{0.5}Mn_{1.5}O_4$

cathode/CM graphite anode) surpasses the challenging value of the long-range EV battery. Furthermore, to visualize this potential advantage of the single-unit HN paper cell for EV applications, we performed a kind of demonstration test using a mini toy car (power required for operation = 6.75 W). Figure 4g shows that the single-unit HN paper cell (weight = 45 mg), which was mounted on top of the toy car roof, operated the toy car for 90 min, which almost corresponded to the energy density of 225 Wh kg^{-1} per cell. Video clips displaying the operation of the toy car were also provided (Supporting Information, Figure S19).

2.4. A Paper Crane HN Cell Fabricated Via Origami Folding Technique

A salient advantage of paper is exceptional deformability (in particular, bendability and foldability),[6] which thus allows a wide range of form factors suitable for various applications in our daily lives. Motivated by this unique feature of paper, shape flexibility of the HN paper cell was investigated, where the CM $LiFePO_4$ cathode (areal mass loading = 7 mg $cm_{cathode}^{-2}$) and CM $Li_4Ti_5O_{12}$ anode (=7.5 mg cm_{anode}^{-2}) were combined with the CNF separator. **Figure 5**a shows that the CM cathode can be folded at an interval of 5 mm. Notably, neither structural disintegration nor detachment of cell components was observed even at the folded edges (Figure 5b). Such excellent flexibility of the CM cathode is due to the CNF/MWNT heteronet-mediated structural tolerance/compliance and also the removal of relatively stiff metallic current collectors. By comparison, a control cathode ($LiFePO_4$/PVdF/carbon black = 80/10/10 (w/w/w) on Al current collector, (areal mass loading = 6 mg $cm_{cathode}^{-2}$) failed to preserve its structural integrity under the same folded state (inset images of Figure 5a,b). Appreciable amounts of cathode components were detached from the Al current collector.

Finally, we fabricated the paper crane HN full cell (=CM $LiFePO_4$ cathode/CNF separator/CM $Li_4Ti_5O_{12}$ anode) using so-called "origami folding skill." The form of paper crane was chosen as a representative example that can demonstrate an extremely folded state of a cell. The stepwise multifolding procedure for making the paper crane HN cell (I) (width × length × thickness = 70 mm × 70 mm × 0.05 mm, before folding) is depicted in Figure 5c. To visualize physical appearance of the paper crane HN cell (I), a polyethylene film (thickness ≈ 100 μm) was used as a transparent packaging substance. Figure 5d shows that the paper crane HN cell (I) successfully operated a light-emitting diode (LED) lamp and also showed stable charge/discharge profiles (at charge/discharge current density of 1.0 C/1.0 C under voltage range of 1.0–2.5 V, Figure S20 (Supporting Information)). In addition, to explore wider applicability of HN paper cells, different type of a paper crane HN cell was fabricated, where the packaging film, together with major cell components, was simultaneously multifolded (Supporting Information, Figure S21). Here, the CM electrodes and CNF separator were packaged with the polyethylene film and then the 2D sheet-shaped cells were subjected to origami folding followed by injection of liquid electrolyte, producing a paper crane HN cell (II). Similar to the previous paper crane HN cell (I) (the polyethylene packaging film was not origami-folded), the new HN cell (II) also successfully lighted up the LED lamp (an inset image of Figure 5d). To further examine such compelling multifoldability, the paper crane HN cell (I) was disassembled, unfolded, injected with liquid electrolyte and finally sealed again. Notably, the unfolded paper crane HN cell (I) also operated the LED lamp (Figure 5e). The above mentioned results on the paper crane HN cells demonstrate that the CNF/MWNT heteronet-based CM electrodes incorporating no metallic current collectors, in combination with the readily deformable CNF separator, bring remarkable advances in the physical flexibility and shape diversity of the cells.

The concept of origami lithium-ion batteries was previously reported by Song et al.[30] However, they used the CNT-coated laboratory Kimwipes paper as a current collector and a polypropylene microporous separator. On top of the Kimwipes paper current collector, conventional electrode slurries (comprising electrode active materials, carbon black powder conductive additives and synthetic polymer binders) were coated. Due to this structural insufficiency, the Kimwipes battery did not deliver the satisfactory level of cell performance (e.g., cell capacity that is affected by mass loading of electrodes). The quantitative comparison in capacity per electrode area (=areal capacity) between the HN paper cells and the previously reported flexible cells[30,31] was presented as a function of bending radius (Figure 5f). The smaller bending radius accounts for the flexibility advancement from "bendable" (via "windable") to "foldable." Over a wide range of bending radius, the HN paper cells showed the superiority in areal capacity than the previous works.

3. Conclusion

In summary, we have demonstrated the CNFs/CNTs-based HN paper batteries as a 1D material-mediated cell architecture strategy to enable ultrahigh energy density and shape versatility far beyond those achievable with conventional battery technologies. The CM electrodes consisted of the CNF/MWNT-intermingled heteronets that embrace electrode active materials, thus offering the well-developed 3D bicontinuous electron/ion transport pathways. Such a novel electrode structure brought significant improvement in the mechanical flexibility, Faradaic reaction kinetics, and electrode mass loading (i.e., areal capacity). More notably, the metallic current collectors-free CNF/MWNT heteronets allowed the multiple stacking of CM electrodes in series, eventually leading to the user-tailored, ultrathick (i.e., high-mass loading) electrodes with reliable electrochemical performance. The multi-stackable CM electrodes were assembled with the CNF separator, leading to the single-unit HN paper cell (composed of one CM cathode/one CNF separator/one CM anode). This single-unit HN paper cell provided an exceptional increase in the energy density (=226 Wh kg^{-1} at 400 W kg^{-1} for $LiNi_{0.5}Mn_{1.5}O_4$/graphite system), which even surpassed the target value (=200 Wh kg^{-1} at 400 W kg^{-1}) of long-range (=300 miles) EV batteries. The (metallic current collectors-free) compliant CM electrodes, in combination with the readily deformable CNF separator, successfully produced the paper crane HN cells via the origami folding technique. We envision that the HN paper batteries based on the 1D building blocks of CNF/MWNT hold a

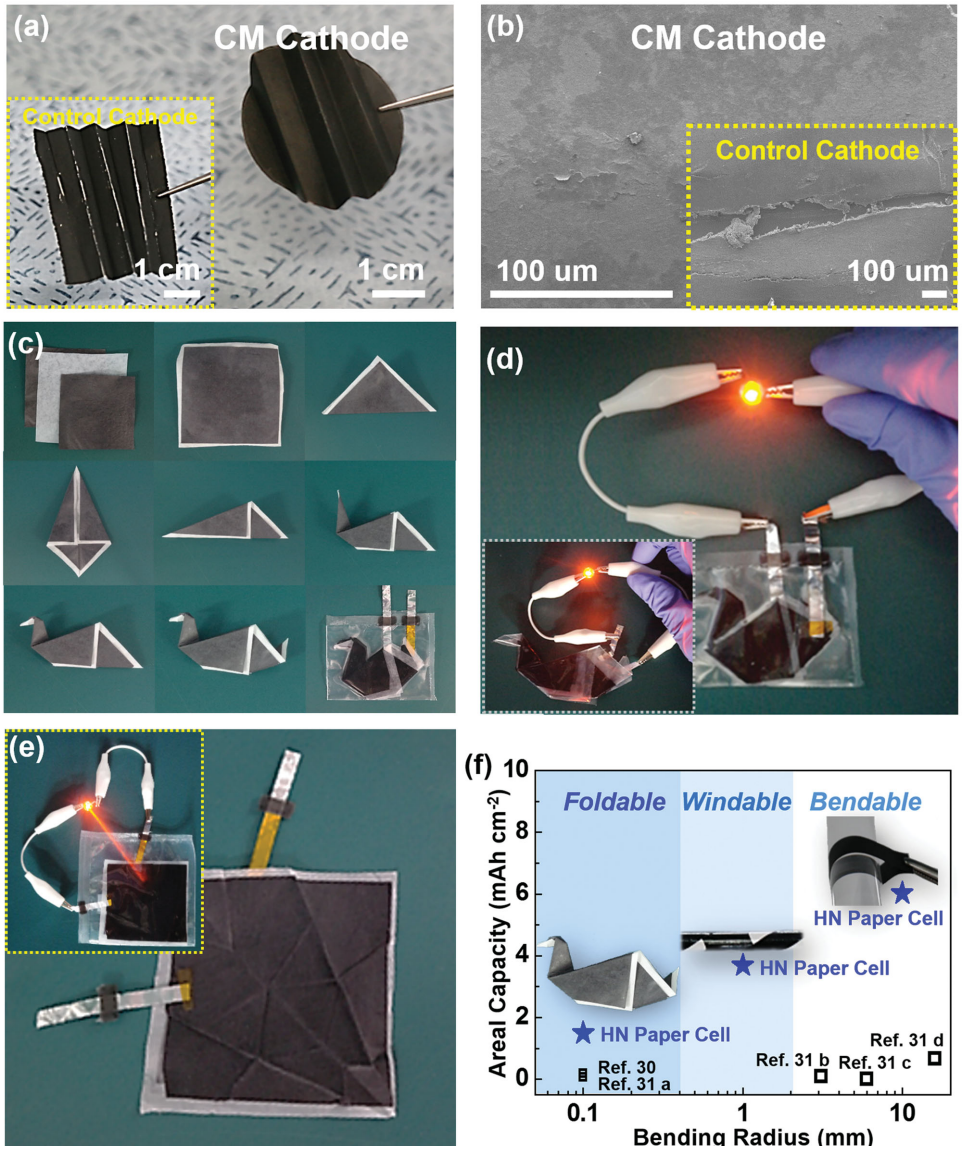

Figure 5. Paper crane HN cells fabricated via origami folding and their electrochemical performance. a,b) Comparison in structural stability between CM $LiFePO_4$ cathode and control $LiFePO_4$ cathode upon multiple folding: a) photographs; b) SEM images (focusing on the folded edges). c) A photograph displaying origami folding-based stepwise multi-folding procedure for making the paper crane HN cell (I). d) Photographs showing the electrochemical activity of paper crane HN cell (I) and paper crane HN cell (II) (an inset image). e) Photographs depicting the electrochemical operation of the unfolded paper crane HN cell (I). f) Comparison in capacity per electrode area (=areal capacity) between the HN paper cells and the previously reported flexible cells as a function of bending radius.

great deal of promise as a cellulose-driven cell platform technology for advanced flexible/high-performance power sources (including new energy storage systems beyond lithium-ion electrochemistry).

4. Experimental Section

Fabrication of CM Electrodes (CNF/MWNT-Intermingled Heteronets Embracing Electrode Active Materials): The CNF suspension was obtained from the repeated high-pressure homogenization of wood cellulose powders (particle size ≈ 45 μm, KC Flock, Nippon Paper Chemicals) in 5 wt% NaOH aqueous solution. The more detailed procedure was described in the previous publications.[10,24] Into the CNF suspension, 1.5 wt% urea was added in order to facilitate the dispersion of CNTs in the CNF suspension. The MWNTs (average diameter = 10–20 nm, average length = 10–20 μm, purity = 90%, CM-130, Hanwha Chemical) were subjected to ultrasonification for 1 h in water, producing well-dispersed MWNT suspension, wherein 1 wt% SDS was incorporated as MWNT-dispersing agent.[15] For the preparation of electrode mixture suspension, electrode active materials ($LiFePO_4$ (Süd Chemie), $Li_4Ti_5O_{12}$ (Aldrich), $LiNi_{0.5}Mn_{1.5}O_2$ (Daejung EM), and Graphite (Sumitomo Metal Industries)) were mixed with the MWNT suspension. Into the MWNT/electrode mixture suspension, the previously prepared CNF suspension containing the urea additive was added dropwise under vigorous stirring at 0 °C, yielding the electrode mixture suspension (i.e., CNF/MWNT/electrode active materials in aqueous solution). Subsequently, the CM electrodes were fabricated through the vacuum-assisted infiltration process analogous to papermaking process. The electrode mixture

suspension mentioned above was poured onto a filter paper positioned inside a Porcelain Buchner funnel and then subjected to the vacuum infiltration, leading to the wet-state CM electrodes. To promote the development of porous structure in the electrodes, the wet-state CM electrodes were subjected to the solvent (ethanol followed by acetone) exchange-assisted freeze drying (freeze dryer (TFD8503, Il Shin BioBase) at –95 °C/5.0 × 10^{-3} Torr for 24 h, eventually producing selfstanding/bendable CM electrodes.

Structural/Physicochemical Characterization of CM Electrodes: The dispersion state of CNF and MWNT suspension was examined with TEM (JEM-2010, JEOL) and X-Ray Diffractometer (D/MAZX 2500V/PC, Rigaku) analysis. The CNFs in the electrode mixture suspension were selectively stained with 0.5% Congo red solution for 3 h and then their dispersion state was observed using opitcal microscopes (FV 1000SPD, Olympus).[19] The surface and cross-sectional morphologies of CM electrodes were investigated by FE-SEM (S-4800, Hitachi) measurement. The porosity of CM electrodes was estimated by measuring their density difference before and after solvent (n-butanol (density = 0.81 g cc^{-1})) uptake. The electronic conductivity of CM electrodes was measured using a 4-probe point technique (CMT-SR1000N, Advanced Instrument Technology). For the electrochemical characterization of CM electrodes, a liquid electrolyte of 1 M $LiPF_6$ in EC/DEC (=1/1 (v/v), Soulbrain) was used. The electrolyte wettability of CM electrodes was quantitatively characterized by measuring their electrolyte immersion-height.

Fabrication and Electrochemical Analysis of HN Paper Cells: The feasibility of HN paper full cells as an alternative power source was explored using unit cells (2032-type coin). All assembly of cells was carried out in an argon-filled glove box. The cell performance was measured using a cycle tester (PNE Solution) at various charge/discharge conditions. The cyclic voltammetry of cells was examined using a potentiostat (VSP classic, Bio-Logic). The overpotential distribution of CM cathodes in the through-thickness direction was investigated using in situ EIS measurement based on electrode-by-electrode stack cell configuration. The electrode-by-electrode stack cell consisted of three cathode layers (thickness of an individual cathode layer = 200 μm) as a working electrode and lithium metal disc as a counter/reference electrode. Polyethylene separators were positioned between each cathode layer to ensure electrical isolation and also allow ionic contact. Meanwhile, to visualize the applicability of the HN paper cells for EV applications, the cell (weight = 45 mg) was mounted on the roof top of a mini toy car (power required for operation = 6.75 W). The operation time of the toy car was measured, which thus allowed us to calculate energy density of the cell.

Origami Foldability of HN Paper Cells: The paper crane HN full cells (composed of CM $LiFePO_4$ cathode/CNF separator/CM $Li_4Ti_5O_{12}$ anode) were fabricated using the origami folding skill. The dimension of the paper crane HN cells was 70 mm × 70 mm × 0.05 mm (width × length × thickness, before folding) and a polyethylene film (thickness ≈100 μm) was used as a transparent packaging substance. After the fabrication of the paper crane HN cells, their charge/discharge behavior was monitored at charge/discharge current density of 1.0 C/1.0 C under voltage range of 1.0–2.5 V.

Supporting Information

Supporting Information is available from the Wiley Online Library or from the author, at the website of the Energy Soft Materials Lab (http://syleek.unist.ac.kr/category/publication/).

Acknowledgements

This work was supported by the Korea Forest Research Institute (Grant No. FP 0400-2007-03) and the Basic Science Research Program through the National Research Foundation of Korea (NRF) funded by the Ministry of Science, ICT and future Planning (2015R1A2A1A01003474).

Received: July 10, 2015
Revised: August 15, 2015
Published online: September 10, 2015

[1] a) M. Armand, J.-M. Tarascon, *Nature* **2008**, *451*, 652; b) M. M. Thackeray, C. Wolverton, E. D. Isaacs, *Energy Environ. Sci.* **2012**, *5*, 7854; c) B. Dunn, H. Kamath, J. M. Tarascon, *Science* **2011**, *334*, 928.

[2] a) B. Scrosati, J. Hassoun, Y.-K. Sun, *Energy Environ. Sci.* **2011**, *4*, 3287; b) G. Jeong, Y.-U. Kim, H. Kim, Y.-J. Kim, H.-J. Sohn, *Energy Environ. Sci.* **2011**, *4*, 1986; c) V. Etacheri, R. Marom, R. Elazari, G. Salitra, D. Aurbach, *Energy Environ. Sci.* **2011**, *4*, 3243.

[3] a) M. S. Whittingham, *Chem. Rev.* **2004**, *104*, 4271; b) M. R. Palacin, *Chem. Soc. Rev.* **2009**, *38*, 2565.

[4] a) K. Evanoff, J. Khan, A. A. Balandin, A. Magasinski, W. J. Ready, T. F. Fuller, G. Yushin, *Adv. Mater.* **2012**, *24*, 533; b) L. Hu, F. La Mantia, H. Wu, X. Xie, J. McDonough, M. Pasta, Y. Cui, *Adv. Energy Mater.* **2011**, *1*, 1012.

[5] a) B. Kang, G. Ceder, *Nature* **2009**, *458*, 190; b) J. B. Goodenough, K.-S. Park, *J. Am. Chem. Soc.* **2013**, *135*, 1167; c) L. Yu, H. B. Wu, X. W. Lou, *Adv. Mater.* **2013**, *25*, 2296.

[6] a) D. Tobjork, R. Osterbacka, *Adv. Mater.* **2011**, *23*, 1935; b) V. L. Pushparaj, M. M. Shaijumon, A. Kumar, S. Murugesan, L. Ci, R. Vajtai, R. J. Linhardt, O. Nalamasu, P. M. Ajayan, *Proc. Natl. Acad. Sci. USA* **2007**, *104*, 13574; c) L. Hu, Y. Cui, *Energy Environ. Sci.* **2012**, *5*, 6423.

[7] a) S. Jeong, N. Böckenfeld, A. Balducci, M. Winter, S. Passerini, *J. Power Sources* **2012**, *199*, 331; b) L. Jabbour, M. Destro, C. Gerbaldi, D. Chaussy, N. Penazzi, D. Beneventi, *J. Mater. Chem.* **2012**, *22*, 3227.

[8] H. Zhu, Z. Jia, Y. Chen, N. Weadock, J. Wan, O. Vaaland, X. Han, T. Li, L. Hu, *Nano Lett.* **2013**, *13*, 3093.

[9] L. Hu, J. W. Choi, Y. Yang, S. Jeong, F. La Mantia, L. F. Cui, Y. Cui, *Proc. Natl. Acad. Sci. USA* **2009**, *106*, 21490.

[10] S.-J. Chun, E.-S. Choi, E.-H. Lee, J. H. Kim, S.-Y. Lee, S.-Y. Lee, *J. Mater. Chem.* **2012**, *22*, 16618.

[11] S. Leijonmarck, A. Cornell, G. Lindbergh, L. Wågberg, *J. Mater. Chem. A* **2013**, *1*, 4671.

[12] a) S. Leijonmarck, A. Cornell, G. Lindbergh, L. Wågberg, *Nano Energy* **2013**, *2*, 794; b) L. Nyholm, G. Nyström, A. Mihranyan, M. Strømme, *Adv. Mater.* **2011**, *23*, 3751; c) K. Jost, C. R. Perez, J. K. McDonough, V. Presser, M. Heon, G. Dion, Y. Gogotsi, *Energy Environ. Sci.* **2011**, *4*, 5060; d) D. I. Choi, H. Lee, D. J. Lee, K.-W. Nam, J.-S. Kim, R. A. Huggins, J.-K. Park, J. W. Choi, *J. Mater. Chem. A* **2013**, *1*, 5320.

[13] H. Zhang, X. Yu, P. V. Braun, *Nat. Nanotechnol.* **2011**, *6*, 277.

[14] K. H. Choi, S. J. Cho, S. J. Chun, J. T. Yoo, C. K. Lee, W. Kim, Q. Wu, S. B. Park, D. H. Choi, S. Y. Lee, S. Y. Lee, *Nano Lett.* **2014**, *14*, 5677.

[15] W. Huang, Y. Lin, S. Taylor, J. Gaillard, A. M. Rao, Y. P. Sun, *Nano Lett.* **2002**, *2*, 231.

[16] a) X. Zhang, Z. Lin, B. Chen, S. Sharma, C.-P. Wong, W. Zhang, Y. Deng, *J. Mater. Chem. A* **2013**, *1*, 5835; b) D. Klemm, F. Kramer, S. Moritz, T. Lindstrom, M. Ankerfors, D. Gray, A. Dorris, *Angew. Chem. Int. Ed.* **2011**, *50*, 5438.

[17] H. Qi, J. Liu, S. Gao, E. Mäder, *J. Mater. Chem. A* **2013**, *1*, 2161.

[18] a) P. Lu, Y.-L. Hsieh, *Carbohydr. Polym.* **2010**, *82*, 329; b) Z. Y. Zhang, I. M. O'Hara, W. O. S. Doherty, *Green Chem.* **2013**, *15*, 431.

[19] J. Verbelen, S. Kerstens, *J. Microsc.* **2000**, *198*, 101.

[20] J. H. Lehman, M. Terrones, E. Mansfield, K. E. Hurst, V. Meunier, *Carbon* **2011**, *8*, 2581.

[21] L.-H. Hu, F.-Y. Wu, C.-T. Lin, A. N. Khlobystov, L.-J. Li, *Nat. Commun.* **2013**, *4*, 1687.
[22] D. W. Dees, S. Kawauchi, D. P. Abraham, J. Prakash, *J. Power Sources* **2009**, *189*, 263.
[23] M. S. Park, S. B. Ma, D. J. Lee, D. Im, S. G. Doo, O. Yamamoto, *Sci. Rep.* **2014**, *4*, 3815.
[24] J.-H. Kim, J.-H. Kim, E.-S. Choi, H. K. Yu, J. H. Kim, Q. Wu, S.-J. Chun, S.-Y. Lee, S.-Y. Lee, *J. Power Sources* **2013**, *242*, 533.
[25] L. Zhou, D. Zhao, X. W. Lou, *Angew. Chem. Int. Ed.* **2012**, *51*, 239.
[26] Z. Yuan, H. J. Peng, J. Q. Huang, X. Y. Liu, D. W. Wang, X. B. Cheng, Q. Zhang, *Adv. Funct. Mater.* **2014**, *24*, 6105.
[27] S. Klink, W. Schuhmann, F. La Mantia, *ChemSusChem* **2014**, *7*, 2159.
[28] N. Kamaya, K. Homma, Y. Yamakawa, M. Hirayama, R. Kanno, M. Yonemura, T. Kamiyama, Y. Kato, S. Hama, K. Kawamoto, *Nat. Mater.* **2011**, *10*, 682.
[29] K. Young, C. Wang, L. Y. Wang, K. Strunz, *Electric Vehicle Integration into Modern Power Networks,* Springer, NY, USA **2013**, pp.15–56.
[30] Z. Song, T. Ma, R. Tang, Q. Cheng, X. Wang, D. Krishnaraju, R. Panat, C. K. Chan, H. Yu, H. Jiang, *Nat. Commun.* **2014**, *5*, 3140.
[31] a) Q. Cheng, Z. Song, T. Ma, B. B. Smith, R. Tang, H. Yu, H. Jiang, C. K. Chan, *Nano Lett.* **2013**, *13*, 4969; b) M. Koo, K.-I. Park, S. H. Lee, M. Suh, D. Y. Jeon, J. W. Choi, K. Kang, K. J. Lee, *Nano Lett.* **2012**, *12*, 4810; c) L. Hu, H. Wu, F. La Mantia, Y. Yang, Y. Cui, *ACS Nano* **2010**, *4*, 5843; d) D. Ge, L. Yang, L. Fan, C. Zhang, X. Xiao, Y. Gogotsi, S. Yang, *Nano Energy* **2015**, *11*, 568.